Proceedings of the 2005 IEEE
International Conference on Robotics and Automation
Barcelona, Spain, April 2005

Polychaete-like Undulatory Robotic Locomotion†

Dimitris P. Tsakiris and Michael Sfakiotakis
Institute of Computer Science – FORTH
Vassilika Vouton, P.O. Box 1385
GR-71110 Heraklion, Greece
{tsakiris, sfakios}@ics.forth.gr

Arianna Menciassi, Gianni La Spina and Paolo Dario
CRIM Lab – Scuola Superiore Sant'Anna
Piazza Martiri della Libertà, 33
56127 Pisa, Italy
{arianna, dario}@sssup.it, giannilaspina@mail-arts.sssup.it

***Abstract* - Polychaete annelid worms provide a biological paradigm of versatile locomotion and effective motion control, adaptable to a large variety of unstructured environmental conditions (water, sand, mud, sediment, etc.). The undulatory locomotion of their segmented body is characterized by the combination of a unique form of tail-to-head body undulations, with the rowing-like action of numerous lateral appendages distributed along their body. Computational models of polychaete-like crawling and swimming have been developed, based on the Lagrangian dynamics of the system and on resistive models of its interaction with the environment, and used for simulation studies demonstrating the generation of undulatory gaits. Several lightweight robotic prototypes have been developed, whose undulatory actuation achieves propulsion on sand. Extensive experiments demonstrate that the propulsion of these robots is characterized by essential features of polychaete locomotion, in agreement with the corresponding simulations.**

Index Terms - biomimetic robotics, undulatory locomotion, motion control, polychaete annelids.

I. Introduction

Locomotion and motion control are among the most significant problems for emerging robotic applications dealing with unstructured and tortuous environments; such applications range from novel diagnostic systems for healthcare (e.g. endoscopic access to the human body) to robotic tools for search-and-rescue operations and to planetary exploration. The human gastrointestinal tract, an earthquake-damaged building or the Martian surface are environments quite different from the usual indoors environments, where most present-day mobile robots operate, and present significant challenges for locomotion. Drawing inspiration from biology, where such problems have been efficiently addressed by the evolutionary process, can help the design of agile robots able to adapt robustly to a variety of environmental conditions; the study of lower animal forms in particular (invertebrates, lower vertebrates) is inspiring robotic locomotion and motion control systems [1-6].

Shape undulations are employed for locomotion by a significant number of organisms, spanning a broad range of body sizes and environmental habitats, since they constitute a satisfactory propulsion mechanism for a wide range of values of the Reynolds number [7]. Particular attention has been devoted by robotics researchers to snake- and eel-like locomotion, leading mostly to wheeled mechanisms for terrestrial locomotion on relatively smooth surfaces (e.g. [4], [8-13]). Recent innovative research efforts on non-wheeled undulatory locomotion bring forth the importance of understanding the interaction of the undulatory mechanism with the environment enabling the locomotion [8],[14-17],[1],[5].

(a) *Nereis virens* (b) *Nepthys hombergi*
Fig. 1: Polychaete annelid worms

An intriguing biological paradigm of locomotion in unstructured environment is offered by a class of segmented marine worms, the polychaete annelids: they can be found living in the depths of the ocean, floating free near the surface, or burrowing in the mud and sand of the seashore. The variety of their morphology, sensory apparatus and nervous system structure is a direct consequence of their adaptation to so diverse habitats (Fig. 1). Their locomotion is characterized by the combination of a unique form of tail-to-head body undulations (opposite direction of propagation than snakes or eels), with the rowing-like action of the numerous active lateral appendages, called parapodia, distributed along their body [18],[19]. Both characteristics provide these worms with distinctive locomotory modes, increasing their terrain traversing and manipulation capabilities and could benefit, if properly replicated, a robotic system.

Sections II and III of the paper describe models of the mechanics and motion control of polychaete undulatory locomotion, as well as associated simulation studies, which demonstrate the generation of polychaete-like undulatory gaits. A series of robotic undulatory prototypes have been developed, which are able of locomotion on sand and other unstructured substrates, and allow the validation and refinement of these models. Section IV describes one of these prototypes, which is used in the experiments. Section V describes robotic experiments of locomotion on sand and compares their results with those of the simulation studies of section III, verifying that, both the robotic prototypes and the related models, are in agreement and capture adequately essential features of polychaete locomotion.

II. Modeling Polychaete Locomotion

A. Equations of Motion

The equations of motion of an undulatory robotic mechanism are obtained from its Lagrangian dynamics, after the reduction process described in [10],[17],[20],[21],[12]

† This work was supported in part by the European Commission, through the Future and Emerging Technologies program (IST-FET), under grant IST-2001-34181 (project BIOLOCH).

and briefly outlined here. A computational model of a planar undulatory mechanism has been developed, based on a serial kinematic chain of *N* rigid links (we consider *N* odd; the case of *N*=7 is shown in Fig. 2). The links are considered to be identical and with the center of mass at the middle of each link. Each of the *N-1* joint angles is considered to be independently actuated, to control the shape of the mechanism.

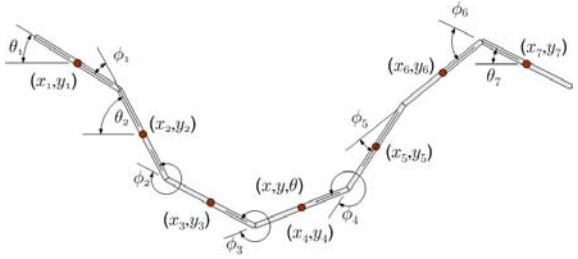

Fig. 2: Multi-segment undulatory mechanism model

The position *(x,y)* and orientation θ of the central link with respect to an inertial coordinate frame on the plane are the system's *group variables* and can be represented by an element g of the group $G = SE(2)$, the Special Euclidean group of order 2. The Lie algebra element, corresponding to g, is $\xi \triangleq g^{-1}\dot{g} \in \mathcal{G} = se(2)$ and describes the *body velocity* of the central link. The joint angle vector $r = (\phi_1, \ldots, \phi_{N-1}) \in \mathcal{S} \triangleq S^{N-1}$ denotes the *shape variables*, $\mathcal{S}$ the *shape space* of the system and S the circle group. From the kinematics of the serial chain, it can be derived that the configuration of the mechanism is $q = (g, r) \in Q = G \times \mathcal{S} \triangleq SE(2) \times S^{N-1}$.

The Euler-Lagrange equations of motion can be reduced by exploiting the invariance of the mechanism to changes in inertial position and orientation, expressed as *Lie group symmetries* exhibited by the system. Assuming the existence of a Lagrangian function $L : TQ \to \mathbb{R}$ and of external forces $F : TQ \to T^*Q$ acting on the system, both of which are invariant under the action of the group *G,* a reduced Lagrangian l can be determined, which is a function of $(r, \dot{r}, \xi)$ and takes the following form in body coordinates:

$$l(r,\dot{r},\xi) = \tfrac{1}{2}\begin{pmatrix}\xi^T & \dot{r}^T\end{pmatrix}\begin{pmatrix}\boldsymbol{I}(r) & \boldsymbol{I}(r)\boldsymbol{A}(r)\\ \boldsymbol{A}^T(r)\boldsymbol{I}(r) & m(r)\end{pmatrix}\begin{pmatrix}\xi^T\\ \dot{r}^T\end{pmatrix}. \qquad (1)$$

The matrix ***A(r)*** is the local form of the *mechanical connection*, and depends only on the shape *r*. The *local locked inertia tensor* ***I(r)*** describes the total inertia of the system, when all joints are frozen at a specific shape configuration *r*. The ***reduced equations of motion*** are, then, obtained in a body-fixed coordinate frame as:

$$\begin{aligned}\dot{g} &= g\,(-\mathbf{A}(r)\dot{\mathbf{r}} + \mathbf{I}^{-1}(r)p)\,,\\ \dot{p} &= ad^*_{\xi}p + \tau_T + \tau_N\,,\\ \tilde{M}(r)\ddot{r} + \dot{r}^T\tilde{C}(r)\dot{r} + \tilde{N} &= B(r)\tau\,,\end{aligned} \qquad (2)$$

where p is the *body momentum,* defined as $p \triangleq \partial l / \partial \xi$; the reduced matrices $\tilde{M}, \tilde{C}, \tilde{N}$ are detailed in [20]; *ad* is the infinitesimal generator of the adjoint action of G on $\mathcal{G}$; τ_T, τ_N are the external frictional forces in the tangential and normal directions of the central link, related to F as described in [20], and are obtained from the frictional force model employed as a function of the tangential and normal velocity of each link (see next subsection). The second equation above describes the evolution of momentum in body coordinates (not conserved in this coordinate frame) and is called the *momentum equation*. The third equation above is a second-order differential equation describing the evolution of the shape variables. The assumption will be made (and investigated experimentally) that full control of the shape variables is possible; therefore, the *controls* of the system are not considered to be the joint torques, but the joint angles *r* themselves. The equations (2) are computationally efficient and well suited to controller development; they are also used to validate the equations of motion derived automatically by the Matlab tools mentioned in section III.B.

B. Interaction with the Environment

Locomotion of an undulating body results from the coupling of its internal shape changes to external motion constraints, usually due to external frictional forces applied through the interaction with the locomotion environment, resisting the motion of body segments. In order to approximate the characteristics of this interaction of the undulatory mechanism described above, with the terrestrial environment (sand, gravel, etc.), viscous damping and Coulomb friction models were considered, as well as extensions of these models that capture phenomena like stiction, anisotropy and the Stribeck effect [22]. They are all of a resistive nature, i.e. the force on each link depends on its velocity (rather than acceleration), and they all involve decoupled force components in the normal and tangential direction of the link's motion. Use of such force models dates back to the analysis of the undulatory swimming of elongate animals in [23] and its variants, which have been applied to both aquatic and terrestrial locomotion.

More specifically, in the viscous damping model, the forces applied in the tangential and normal directions of the *i*-th link's motion are linearly dependant on the respective velocity components, i.e. $F_T^i = -c_T v_T^i$ and $F_N^i = -c_N v_N^i$, where c_T and c_N are the viscous friction coefficients in the tangential and normal directions, respectively. Alternatively, the Coulomb friction model can be used to model non-viscous interaction with the environment, where the applied frictional force depends only on the direction of the link's velocity, rather than on its magnitude: $F_T^i = -\mu_T gm \cdot sgn(v_T^i)$, $F_N^i = -\mu_N gm \cdot sgn(v_N^i)$, where μ_T and μ_N are the Coulomb friction coefficients, m is the mass of the link and g is the constant of gravity. The values of the friction coefficients in both models depend on the configuration of the contact surface (the underside of the links forming the undulatory mechanism), as well as the material properties of the locomotion environment.

In all of the above friction models, the ratio of the friction coefficients is a key parameter in undulatory locomotion, which, to a large extent, determines the stride length (distance traveled per undulation cycle) for a given body wave, as well as the direction of motion of the undulatory locomotor with respect to the direction of its shape wave. This may be seen in the context of aquatic locomotion, where, to a first approximation, the fluid drag forces are $F_T^i = -\lambda_T sgn(v_T^i)\left|v_T^i\right|^2$ and $F_{\mathrm{N}}^i = -\lambda_{\mathrm{N}} sgn(v_{\mathrm{N}}^i)\left|v_{\mathrm{N}}^i\right|^2$

(see [24] for the assumptions and limitations involved). The elongated body of anguilliform swimming animals (e.g. eels) is smooth and of elliptical cross-section, so that the fluid drag coefficient in the normal direction is significantly greater than the tangential one ($\lambda_N > \lambda_T$). The overall locomotion direction is then opposite to that of the wave direction, and therefore, forward propulsion is achieved by body waves propagating from head to tail; moreover, smooth elongated animals can swim backwards by reversing the propulsive wave [23]. If the animal body is not smooth, the propulsive component of the tangential force may be greater than that of the normal force (corresponding to $\lambda_T > \lambda_N$), and locomotion is along the direction of wave propagation. Forward motion would then be achieved by a tail-to-head wave. This is indeed the case for the locomotion of errant polychaete, whose body affords a significant amount of roughness, mainly due to their parapodia [23]. In general, the larger the differential between the normal and the tangential friction coefficients is, the larger the stride length attainable for a given body wave [24]. These general characteristics also apply to the Coulomb and the viscous damping models.

Research efforts in undulatory robotics have considered the case where resistance in the normal direction of link motion is significantly higher than resistance in the tangential direction, resulting in devices that propel themselves by head-to-tail body waves (e.g. [4],[8],[9],[11], [14],[16],[17]). Apart from presenting a novel robotic prototype moving by tail-to-head waves, this paper also attempts to bring forth the significance of exploiting the interaction with the environment, in designing efficient undulatory mechanisms.

III. Motion Control and Gait Generation

A. Undulatory Gait Generation

The most straightforward way to generate a travelling wave in a serial chain of N links is by having the joint angles vary sinusoidally, with a common frequency f and a constant phase lag φ_{lag} between consecutive joints:

$$\varphi_i(t) = A\sin\left(2\pi ft + i\varphi_{lag}\right) - \psi, \qquad 1 \le i < N, \tag{3}$$

where A is the maximum angular deflection for each joint. The angular offset ψ provides a means for steering the mechanism, and is set to $\psi = 0$ for locomotion in a straight line. If ψ is non-zero, the mechanism moves along a curved path, clockwise or counter-clockwise, depending on the sign of the offset. Depending on the type of interaction with the locomotion environment, the generated body wave will propel the mechanism either in the direction of propagation of the body wave (polychaete-like) or in the opposite direction (eel-like). The wave propagation direction depends on the sign of the phase lag parameter, and is from link-N to link-1 for $\varphi_{lag} > 0$; if this wave propagation direction results in forward motion, then reversing this sign results in backwards motion. The condition $\varphi_{lag} = \pm 2\pi/N$ yields (exactly) one wavelength of the propulsive wave across the undulating body, with beneficial effects on the propulsive efficiency. Varying the joint angle amplitude A affects the wavelength and propagation velocity of the body wave.

Variations of (3) can be used to obtain additional gaits for an undulatory mechanism. More specifically, in-place rotation can be achieved by:

$$\varphi_i(t) = \begin{cases} A\sin\left(2\pi ft + (i-M)\varphi_{lag}\right) - \psi, & 1 \le i \le M, \\ A\sin\left(2\pi ft + (M+1-i)\varphi_{lag}\right) + \psi, & M < i < N, \end{cases} \tag{4}$$

where $M = (N-1)/2$ (for N odd) is the index of the central link. Similarly, a parallel-parking gait is obtained by inverting the sign of the offset in (4) for $1 \le i \le M$.

A biomimetic neuromuscular motion control scheme, based on central pattern generators to generate the body travelling wave via joint torque control, is outlined in [5].

B. Simulation Studies of Undulatory Gaits

In order to facilitate the construction of models of undulatory robots and the analysis of their locomotion, a simulation environment has been developed [24]. It is based on the Matlab/Simulink™ suite and its SimMechanics physical modeling toolbox. It is composed of libraries of elementary "body segment" blocks, which are connected to simulate the mechanics and control of planar articulated robots, by deriving automatically and solving the equations of motion.

This simulation environment has been used to create a computational model of the eleven-link robotic prototype presented in the next section. The Coulomb friction model, with $\mu_N = 0.73$ and $\mu_T = 0.88$, which reflects the experimental conditions on fine sand presented in the next section, is used to model the interaction with the specific substrate.

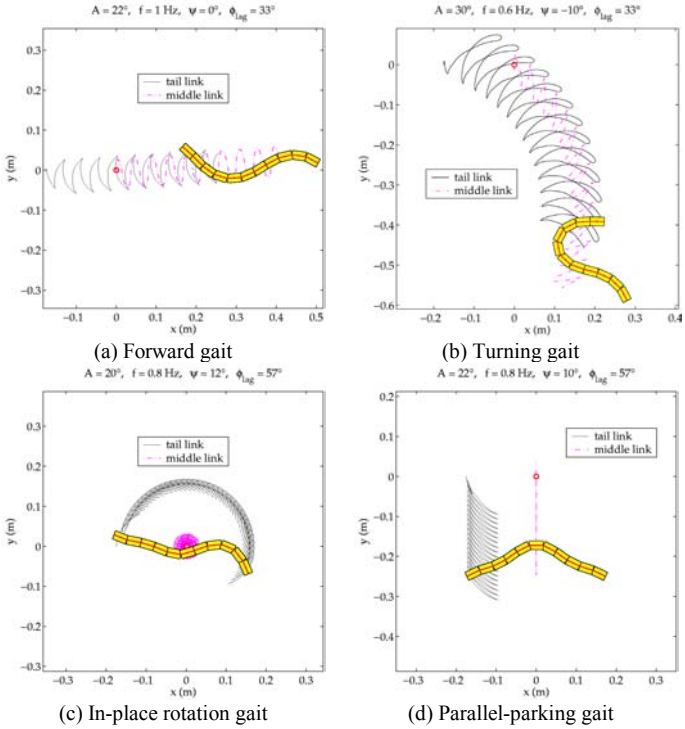

(a) Forward gait (b) Turning gait

(c) In-place rotation gait (d) Parallel-parking gait

Fig. 3: Simulations of undulatory gaits. At t=0, the mechanism is aligned with the x-axis and the center of the middle link is located at point (0,0).

The undulatory gaits of (3)-(4) have been implemented in simulation using this robot configuration; indicative trajectories are shown in Fig. 3. Polychaete-like undulatory trajectories present a number of characteristics differentiating them from the more widely studied eel-like ones. These include the sickle-like shape of the tail link's trajectory in forward motion (Fig. 3(a)), as well as the fact that, during turning, the mean path of distal links has a distinct offset from the mean path traced by the middle link (Fig. 3(b)).

The effect of the joint amplitude A and joint frequency f on the locomotion of the undulatory mechanism is important for altering the mean heading speed. This effect can be characterized, for the forward gait, in terms of the stride length, and is shown in Fig. 4(a) for a range of A and f values, demonstrating that it depends primarily on A. Related results for the mean heading speed itself can be seen in Fig. 8.

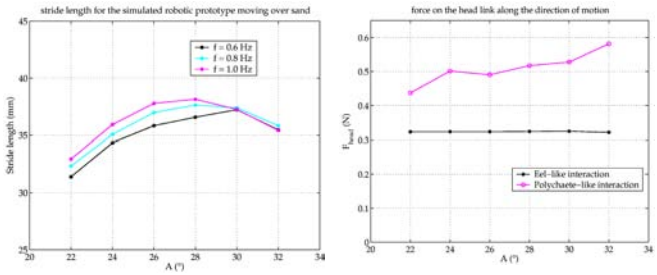

(a) Stride length (b) Average force on the head link

Fig. 4: Simulation studies

Of particular interest, for the intended applications of the robotic locomotors considered, is their potential for burrowing, a common activity among polychaete. The tail-to-head body wave is thought to assist these animals in penetrating the substrate. The effectiveness of utilising tail-to-head body waves for burrowing, compared to utilising head-to-tail ones, was studied by simulations; these used the 11-link mechanism with viscous friction, considering both polychaete-like ($c_N=1$ and $c_T=10$) and eel-like ($c_N=10$ and $c_T=1$) interaction with the environment (cf. discussion in section II.B). They were performed over a range of f and A values, each time using the same body wave for the two configurations. In order to characterize burrowing potential, the average force generated on the "head" link of the mechanism, along the mean direction of motion, was calculated, since the "head" link appears to play the most significant role, among all links, in penetrating the substrate. Results in Fig. 4(b) indicate that greater forces are consistently generated on the "head" link when forward locomotion is by polychaete-like tail-to-head body waves.

C. Simulation Studies Involving Parapodia

The combination of body undulations and parapodial action, in polychaete annelids, offers significant advantages on unstructured substrates (extra gaits, better adaptation and adhesion to local environment). The simulation studies presented earlier were extended to mechanisms equipped with active lateral appendages, akin to the polychaete parapodia (Fig. 5(a)), in order to investigate their potential for improved terrain traversability and maneuverability. In these mechanisms (as in their natural counterparts), the tail-to-head body wave (3) is coupled to periodic movements of the parapodia. These are performed with the same frequency of oscillation f as the body wave, and timed so that their power stroke occurs when they are at its crest [18]: $\zeta_i = -(\pi/2) + C\,c_i$, $\chi_i = (\pi/2) + C\,c_i$, for $1 \le i < N$, where C is the parapodium joint angle amplitude, determining the extent of its sweeping motion, and $c_i \triangleq \cos(2\pi ft + i\varphi_{lag})$.

For simulations of terrestrial locomotion, the interaction of the parapodia with the substrate is approximated using Coulomb friction, taking into account the fact that forces are only generated during a short period of their oscillation cycle (for χ_i and ζ_i in the region of $\pi/2$) and are lifted off the ground during the remaining time [18],[19].

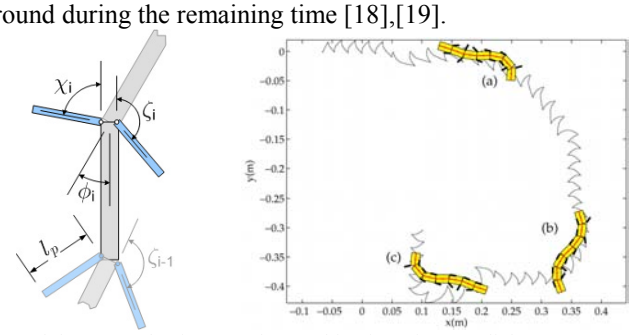

(a) Undulatory mechanism with parapodial links (b) Combination of parapodial movements with body undulations

Fig. 5: Simulation studies involving parapodial links

The extended maneuverability afforded by incorporating the parapodia is demonstrated in Fig. 5(b) by a 7-link mechanism equipped with 6 pairs of parapodial appendages. A series of 90° orientation changes are performed by various combinations of body undulatory gaits and parapodial action: (a) by the turning gait (angular offset $\psi=15°$), while the parapodia move on both sides, (b) by the forward gait ($\psi=0°$), while the parapodia are disabled on one side of the body, and (c) by the turning gait ($\psi=15°$), while the parapodia are again disabled on one side of the body. The reduced time and turning radius for performing the reorientation maneuver in this last case is evident from the trace of the tail link trajectory in Fig. 5(b).

IV. Undulatory Robotic Prototypes

Several polychaete-like robotic prototypes have been developed (currently without parapodial appendages), to allow validation of the computational models and in-depth analysis of the interaction with unstructured substrates. The lightweight eleven-link prototype used in this work (Fig. 6(a)) was built using traditional fabrication technologies and off-the-shelf components. Its total length is 38 cm and total weight is 360 g. Each segment is 35 mm long and is composed of a servomotor, which actuates one of the ten rotary degrees of freedom of the mechanism, and an aluminium case. A Visual Basic® user interface has been developed to facilitate the real-time setting of the body wave parameters.

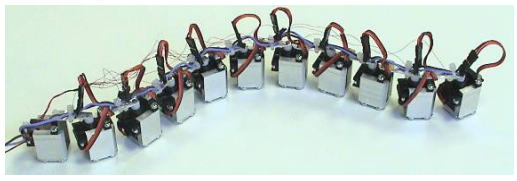

(a) The 11-link, 10-dof undulatory robotic prototype

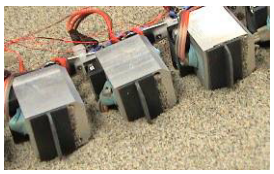

(b) Single-blade SCM mounted transversally to the segment

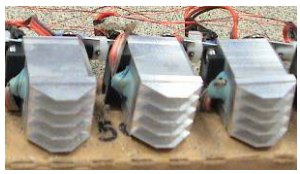

(c) Multi-blade SCM mounted longitudinally to the segment

Fig. 6: The 11-link undulatory robotic prototype.

The underside of each segment is in contact with the substrate and is responsible for the generation of appropriate frictional forces in the tangential and normal segment directions, leading to the different locomotion gaits presen-

ted earlier. This is built as a detachable component of each segment and is called the Segment Contact Module (SCM). Two types of SCMs were developed and tested: the first one exploiting a single blade of Delrin®, and the second made of five stiff aluminium blades (Fig. 6(b), (c)). Each one of these can be mounted either transversally or longitudinally with respect to the main axis of the segment.

The friction characteristics of the segments need to be measured, for a given locomotion environment, in order to introduce the correct friction parameters into the simulations. For the experiments presented here, fine sand was selected as the locomotion substrate. Table I summarizes the results of the friction coefficient measurements (frictional force divided by *mg*, where *m* is the segment mass) for single- and multi-blade SCMs, when the blades are parallel (//) to the traction direction and when they are perpendicular (⊥) to it. It can be seen that, for both SCM designs, the frictional forces generated show a relatively small variance with traction velocity. Therefore, a Coulomb friction model can be used as a first approximation of the interaction of the robot with the sand.

TABLE I

	Single-blade SCM		**Multi-blade SCM**	
	//	⊥	//	⊥
Static friction	1.08	1.18	1.09	1.22
(mm/s)	**Dynamic friction**			
V_1 = 5.8	0.73	0.85	0.93	1.15
V_2 = 8.0	0.68	0.85	0.96	1.07
V_3 = 11.0	0.71	0.89	0.84	1.12
V_4 = 13.4	0.76	0.91	1.07	1.26
V_5 = 18.2	0.77	0.92	0.97	1.19
Mean	0.73	0.88	0.95	1.15

In order to obtain polychaete-like frictional contact, where the tangential friction is higher than the normal one, the SCM units were placed, following the results of Table I, so that their blades are transverse to the main axis of the link, both for single-blade and for multi-blade SCMs (cf. Fig. 6(b)). With these experimental conditions, the perpendicular direction results (⊥) of Table I correspond to tangential friction, while the parallel ones (//) to normal friction.

V. Experiments On Sand

A. The Experimental Setup

A series of experiments was performed in order to assess the capability of the prototype to generate polychaete-like undulatory gaits on sand. The prototype was placed inside a box (size: 1 m x 0.7 m), which was uniformly filled with 20 mm of fine sand (mean diameter of particles equal to 0.56 mm). During the robot movement, the SCM blades were never in contact with the bottom of the box.

Robot trajectory data during test runs were obtained using a 3D localizer able to acquire in real time the position of several light spots (infrared emitters on the robot).

B. Experiments of Undulatory Gait Generation on Sand

The control laws of section III are applied to the 11-link robotic prototype moving on sand, to produce the four main undulatory gaits presented in section III.B. Representative results from these experiments are shown in Fig. 7, both in terms of pictures of the traces left by the robot as it moves on the sand (on the right) and in terms of trajectory plots of a single link generated from the 3D localizer data (on the left). In Fig. 7(e), (f), the robot moves from left to right using the forward and turning gaits (the robot length in these pictures can be used as an indication of the distance travelled; this distance is shown explicitly on the individual link trajectory plots of Fig. 7(a), (b)). Backwards movement is obtained simply by reversing the body wave direction, e.g. by inverting the sign of φ_{lag} in (3) or (4). In Fig. 7(g), the robot rotates clockwise by more than π *rad* using the in-place rotation gait (tail link trajectory plot in Fig. 7(c)). In Fig. 7(h), the robot moves downwards, laterally to its longitudinal axis, using the parallel-parking gait (central link trajectory plot in Fig. 7(d)).

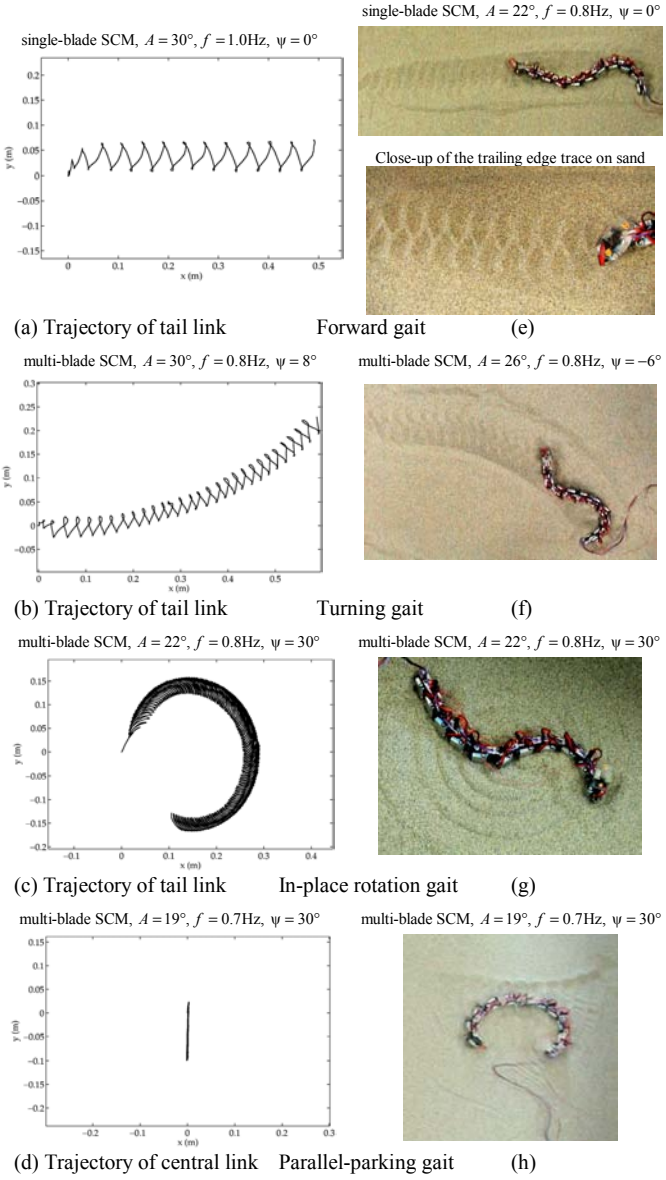

(a) Trajectory of tail link — Forward gait — (e)

(b) Trajectory of tail link — Turning gait — (f)

(c) Trajectory of tail link — In-place rotation gait — (g)

(d) Trajectory of central link — Parallel-parking gait — (h)

Fig. 7: Experimental results demonstrating polychaete-like undulatory gait generation on sand: (a-d) Representative link trajectories, (e-h) Image stills. In all instances, the initial position of the robot is along the x-axis.

Significant qualitative agreement can be observed between the trajectory plots of the robot links in Fig. 7 and the corresponding simulation results in Fig. 3. The sickle-like trajectory of the tail link seen in the forward gait (Fig. 7(a), (e)) is similar to the one obtained in simulation (Fig. 3(a)). In Fig. 7(e), (f), the robot can be seen to dig a small trench, as it propels itself forward, while, simultaneously,

displacing the sand (a form of burrowing). This is particularly pronounced during the turning gait (Fig. 7(f)), where, as mentioned in section III.B, the paths of distal links have a relative offset (Fig. 3(b)): the lower part of the trench seen in this picture is due to the tail link, while the upper part is due to the head.

The main undulatory gaits were successfully generated for both single- and multi-blade SCMs; also, using coarser sand as a substrate (mean particle diameters up to 5.32 mm) and using other similar undulatory robotic prototypes.

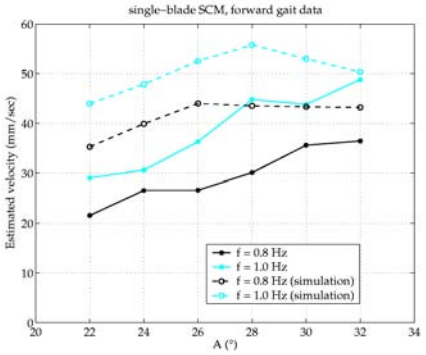

Fig. 8: Experimental estimates of the mean velocity of the robotic prototype for the undulatory forward gait (solid lines), compared with corresponding simulation results (dashed lines).

The trajectory data from the forward gait experiments were analyzed to estimate the stride lengths S_L achieved with the robot. The mean velocity for each experiment was subsequently estimated as $f\,S_L$, for the frequency f used. The results are summarized in Fig. 8, where it is confirmed that higher velocities are associated with increased values for A and f. In experiments with even higher values of A and f, the actuators were reaching their output torque limits, which typically led to the implementation of a body wave with reduced amplitude; these torque limits did not affect significantly the oscillation frequency. As can be easily observed from Fig. 8, the mean velocities achieved by the robot (70-180 m/h) show good agreement with the ones obtained in simulation. This indicates that the computational models developed here capture adequately the dominant characteristics of the interaction with the environment.

VI. Conclusions

This paper presents a series of biomimetic robots, inspired from the morphology and locomotion of the polychaete annelid worms, and studies, both experimentally and in simulation, the undulatory locomotion of these robots on sand. To the best of the authors' knowledge, this is the first work on undulatory robotic locomotion, which considers propulsion and motion control on such a substrate, without the help of wheels or tracks.

Apart from the results presented here, evidence was obtained during these experiments that this mode of robotic locomotion performs well on different types of sand, and over a wide range of robot sizes, from the ones presented here to robots whose size is one order of magnitude less.

Future work will explore further this mode of locomotion on other unstructured substrates (mud, gavel, etc.), the coupling of body undulations with parapodia, and the use of sensory information in closed-loop motion control schemes.

Acknowledgment

D.P.T. thanks P.S. Krishnaprasad and J.F.V. Vincent for insightful discussions. The authors thank the members of the CVRL group of ICS-FORTH, and G. Pernorio, V. Mattoli and O. Tonet, for their technical assistance, as well as the BIOLOCH consortium for their contributions. Related papers and videos of the experimental results presented here can be found at the Web site *www.ics.forth.gr/bioloch*.

References

[1] J. Ayers, J.L. Davis, and A. Rudolph (Eds.), *Neurotechnology for Biomimetic Robots*, MIT Press, 2003.

[2] A. Menciassi and P. Dario, "Bio-inspired solutions for locomotion in the gastrointestinal tract: background and perspectives," *Phil. Trans. - Math., Phys. & Eng. Sciences A*, vol. 361, pp. 2287-2298, 2003.

[3] A. Menciassi, S. Gorini, G. Pernorio, and P. Dario, "A SMA Actuated Artificial Earthworm," Proc. *IEEE Int. Conf. Robotics and Automation (ICRA'04)*, New Orleans, USA, pp. 3282-3287, 2004.

[4] S. Hirose, *Biologically Inspired Robots: Snake-Like Locomotors and Manipulators*, Oxford University Press, 1993.

[5] D.P. Tsakiris, A. Menciassi, M. Sfakiotakis, G.L. Spina, and P. Dario, "Undulatory locomotion of polychaete annelids: mechanics, neural control and robotic prototypes," presented at *The Annual Computational Neuroscience Meeting*, Baltimore, USA, 2004.

[6] M.H. Dickinson, C.T. Farley, R.J. Full, M.A. Koehl, R. Kram, and S. Lehman, "How animals move: an integrative view," *Science*, vol. 288, pp. 100-106, 2000.

[7] J. Lighthill, *Mathematical Biofluiddynamics*, SIAM, 1975.

[8] S. Hirose and E.F. Fukushima, "Snakes and strings: New robotic components for rescue operations," *Int. J. Robot. Res.*, vol. 23, pp. 341-349, 2004.

[9] J. Ostrowski and J. Burdick, "The geometric mechanics of undulatory robotic locomotion," *Int. J. Robot. Res.*, vol. 17, pp. 683-701, 1998.

[10] A.M. Bloch, P.S. Krishnaprasad, J.E. Marsden, and R.M. Murray, "Nonholonomic mechanical systems with symmetry," *Arch. Ration. Mech. Anal.*, vol. 136, pp. 21-99, 1996.

[11] S.D. Kelly and R.M. Murray, "Geometric phases and robotic locomotion," *J. Rob. Syst.*, vol. 12, pp. 417-431, 1995.

[12] P.S. Krishnaprasad and D.P. Tsakiris, "Oscillations, SE(2)-snakes and motion control: a study of the Roller Racer," *Dyn. Syst.*, vol. 16, pp. 347-397, 2001.

[13] P.S. Krishnaprasad and D.P. Tsakiris, "G-Snakes: nonholonomic kinematic chains on Lie groups," Proc. *33rd IEEE Conf. Decision and Control*, Lake Buena Vista, USA, pp. 2955-2960, 1994.

[14] M. Saito, M. Fukaya, and T. Iwasaki, "Modeling, analysis, and synthesis of serpentine locomotion with a multilink robotic snake," *IEEE Contr. Syst. Mag.*, vol. 22, pp. 64-81, 2002.

[15] S.D. Kelly and R.M. Murray, "Modelling efficient pisciform swimming for control," *Int. J. Robust and Nonlinear Control*, vol. 10, pp. 217-241, 2000.

[16] K.A. McIsaac and J.P. Ostrowski, "A geometric approach to anguilliform locomotion: modeling of an underwater eel robot," Proc. *IEEE Int. Conf. Robotics and Automation (ICRA'99)*, pp. 2843-3848, 1999.

[17] J. Cortes, S. Martinez, J.P. Ostrowski, and K.A. McIsaac, "Optimal gaits for dynamic robotic locomotion," *Int. J. Robot. Res.*, vol. 20, pp. 707-728, 2001.

[18] J. Gray, *Animal Locomotion*, Norton, 1968.

[19] R.C. Brusca and G.J. Brusca, *Invertebrates*, Sinauer Associates, 1990.

[20] R.M. Murray, "Nonlinear control of mechanical systems: a Lagrangian perspective," *Annu. Rev. Control*, vol. 21, pp. 31-42, 1997.

[21] J.E. Marsden and T.S. Ratiu, *Introduction to Mechanics and Symmetry*, Springer Verlag, 1994.

[22] H. Olsson, K.J. Astrom, C.C. de Witt, M. Gafvert, and P. Lischinsky, "Friction models and friction compensation," *Eur. J. Control*, vol. 29, pp. 176-195, 1998.

[23] G. Taylor, "Analysis of the swimming of long and narrow animals," *Proc. Royal Society (A)*, vol. 214, pp. 158-183, 1952.

[24] M. Sfakiotakis and D.P. Tsakiris, "A simulation environment for undulatory locomotion," Proc. *IASTED Int. Conf. Applied Simulation and Modelling (ASM2004)*, Rhodes, Greece, pp. 154-159, 2004.